



## Investigation of iron emission lines in the eclipsing high mass X-ray binary pulsar OAO 1657-415

Gaurava K. Jaisawal<sup>1\*</sup> and Sachindra Naik<sup>1†</sup>

<sup>1</sup>Physical Research Laboratory, Navrangapura, Ahmedabad 380009, Gujarat, India

Received 2014 August 13; accepted 2014 December 01

**Abstract.** We present the results obtained from timing and spectral studies of high mass X-ray binary pulsar OAO 1657-415 using a *Suzaku* observations in 2011 September. X-ray pulsations were detected in the light curves up to  $\sim 70$  keV. The continuum spectra during the high- and low-flux regions in light curves were well described by high energy cutoff power-law model along with a blackbody component and iron fluorescent lines at 6.4 keV and 7.06 keV. Time resolved spectroscopy was carried out by dividing the entire observations into 18 narrow segments. Presence of additional dense matter at various orbital phases was confirmed as the cause of low-flux regions in the observations. Presence of additional matter at several orbital phases of the pulsar was interpreted as due to the inhomogeneously distributed clumps of matter around the neutron star. Using clumpy wind hypothesis, the physical parameters of the clumps causing the high- and low-flux episodes in the pulsar light curve were estimated. The equivalent width of iron emission lines was found to be significantly large at certain orbital phases of low-flux segments. We investigated the iron line emitting regions and suggest the existence of neutral and ionized iron atoms in emission sites that are located within the accretion radius.

*Keywords* : pulsars: general – stars: individual (OAO 1657-415) – stars: neutron

### 1. Introduction

Accretion powered high mass X-ray binary pulsar OAO 1657-415 was discovered by Copernicus satellite (Polidan et al. 1978). Initially, the object was incorrectly identified with the massive binary V861 Sco and the system interpreted as a black hole binary. However, the observations with

---

\*email: gaurava@prl.res.in

†email: snaik@prl.res.in

HEAO 1 and Einstein observatories were used to determine the precise position of the source that ruled out V861 Sco as the companion of OAO 1657-415. Using the same data, a pulsation period of 38.22 s was detected in the pulsar (White & Pravo 1979; Parmar et al. 1980). Long-term monitoring of the pulsar with the Burst and Transient Source Experiment (BATSE) onboard Compton Gamma Ray Observatory (CGRO) confirmed the system as an eclipsing binary (Chakrabarty et al. 1993). The orbital parameters derived from the BATSE observations are: orbital period  $P_{orb} = 10.444 \pm 0.004$  d, duration of the eclipse = 1.7d,  $e = 0.104 \pm 0.005$ ,  $a_x \sin i = 106 \pm 0.5$  lt-sec and  $\omega = 93^\circ \pm 5^\circ$ . Using these orbital parameters, the mass and radius of companion were estimated to be in the range of 14–18  $M_\odot$  and 25–32  $R_\odot$ , respectively (Chakrabarty et al. 1993). However, the counterpart was not detected at the *Chandra* position of the pulsar in the deep optical imaging of the field with a limitings magnitude of  $V < 23$ , near infrared (NIR) imaging revealed a highly reddened B-type supergiant star as binary companion of OAO 1657-415 (Chakrabarty et al. 2002). The distance of binary system was estimated to be  $6.4 \pm 1.5$  kpc. On the basis of NIR spectroscopy, the spectral class of the binary companion was refined as Ofpe/WNL type star (Mason et al. 2009). Such stars are known to be the transitional objects between the main sequence and Wolf-Rayet stars.

In high mass X-ray binary (HMXB) systems, mass transfer occurs from the binary companion to the neutron star through the capture of stellar wind, accretion through the Be circumstellar disk or the Roche lobe overflow. Based on the mechanism of mass accretion, the supergiant X-ray binaries (SGXBs; a subclass of HMXBs) are classified into disk-fed and wind-fed SGXB. HMXBs exhibit a definite positions in the spin period versus orbital period diagram (Corbet 1986) depending on the type of mass accretion. The wind-fed SGXBs are distributed in the form of horizontal line in Corbet diagram with exceptions of OAO 1657-415 and 2S 0114+65. However, the three known disk-fed SGXBs such as Cen X-3, SMC X-1 and LMX X-4 show anti-correlation between spin and orbital period. The moderate values of spin and orbital period of OAO 1657-415 make the pulsar as an unique transitional source from wind-fed to disk-fed SGXB.

Spin period evolution of OAO 1657-415 was studied by using *BATSE* and *Rossi X-ray Timing Explorer (RXTE)* observations (Baykal 1997; Bildsten et al. 1997; Baykal 2000). *BATSE* observations of the pulsar revealed strong and stochastic variability in the spin period of the pulsar. Alternating steady spin-up and spin-down episodes lasting for 10–200 d, as seen in Cen X-3, were detected in OAO 1657-415 (Bildsten et al. 1997). These episodes of frequent torque reversals cannot be explained only by wind accretion, rather possibility of the formation of a temporary accretion disk was considered to explain the observed changes in spin period history (Baykal 1997). *RXTE* observations of the pulsar in 1997 August covering a binary orbit showed an extended spin-down episode (Baykal 2000). During these observations, a marginal correlation was seen between X-ray luminosity and change in the pulse frequency of the pulsar. This positive correlation suggested that the disc formed in the spin-down episode is in the prograde direction. Study of the pulse frequency history of OAO 1657-415 by using nearly 19 years of data obtained from *BASTE* and *Gamma-Ray Burst Monitor (Fermi/GBM)* observations inferred the occurrence of two modes of accretion in the pulsar. Presence of a stable accretion disk was suggested during

flux correlated steady spin-up episodes (disk wind accretion) whereas the other type is during flux uncorrelated spinning down of the pulsar at a lesser rate (wind accretion) (Jenke et al. 2012).

The pulsar being at low galactic latitude, the X-ray spectrum shows significant photoelectric absorption at soft X-rays with an equivalent hydrogen column density of  $\geq 10^{23}$  atom  $\text{cm}^{-2}$  (Parmar et al. 1980). However, *Ginga* observations of the pulsar showed the presence of soft X-ray excess below  $\sim 3$  keV (Kamata et al. 1990). Apart from the soft X-ray excess, an iron fluorescence emission line at  $\sim 6.6$  keV was also detected in the *Ginga* spectrum of the pulsar. *ASCA* observation of the pulsar near mid-eclipse time revealed that though the continuum was weak, the 6.4 keV iron fluorescent emission line was dominant compared to 6.7 keV. Another long *ASCA* observation covering non-eclipse through mid-eclipse phase of the pulsar showed that the out-of-eclipse high intensity spectrum had an absorbed continuum component along with 6.4 keV and 7.06 keV iron emission lines (Audley et al. 2006). Broad-band spectrum of the pulsar in 1.0-100 keV energy range, obtained from *BeppoSAX* observation, was found to be well described by a cutoff power law or power-law modified by a high energy cutoff continuum model along with an iron fluorescence line at 6.5 keV (Orlandini et al. 1999). Also there was a hint of the presence of a cyclotron absorption feature at  $\sim 36$  keV as required by one of the above continuum model, the absence of such feature in the model independent Normalized Crab ratio - a technique used to identify cyclotron scattering resonance features in the spectra of X-ray pulsars - made the detection inconclusive (Orlandini et al. 1999). *INTEGRAL* observations also did not find any signature of the cyclotron absorption features in the broad-band (6-200 keV range) spectrum of OAO 1657-415 (Barnstedt et al. 2008).

For a detailed study of the characteristics properties of iron emission lines and broad-band spectral properties, the eclipsing HMXB pulsar OAO 1657-415 was observed with *Suzaku* on 2011 September 26. Though this observation was recently used to describe the timing and spectral properties of the pulsar (Pradhan et al. 2014), we investigated the properties of iron emission lines at different orbital phases of the pulsar and tried to interpret the results by applying clumpy wind model. The results obtained from our study are described in the paper.

## 2. Observations

*Suzaku*, the fifth Japanese X-ray astronomy satellite, was launched by Japan Aerospace Exploration Agency (JAXA) on 2005 July 10 (Mitsuda et al. 2007). It covers very wide energy range (0.2-600 keV) with two sets of detectors, X-ray Imaging Spectrometer (XIS; Koyama et al. 2007) and Hard X-ray Detector (HXD; Takahashi et al. 2007). Three front illuminated (XIS-0, XIS-2, XIS-3) and one back illuminated (XIS-1) CCD detectors are located at focal point of their respective X-ray telescopes. Field of view (FoV) of XIS is  $17'.8 \times 17'.8$  in full window mode. Effective areas of front illuminated and back illuminated detectors in full window mode are  $340 \text{ cm}^2$  and  $390 \text{ cm}^2$  at 1.5 keV, respectively. HXD detector comprises of two sets of instruments - PIN and GSO. PIN is silicon diode detector working in 10-70 keV energy range whereas GSO is scintillator detector that covers 40-600 keV energy range. The effective areas for PIN and GSO are  $145 \text{ cm}^2$  at 15 keV and  $315 \text{ cm}^2$  at 100 keV, respectively. FoV of PIN and GSO (below 100 keV) is

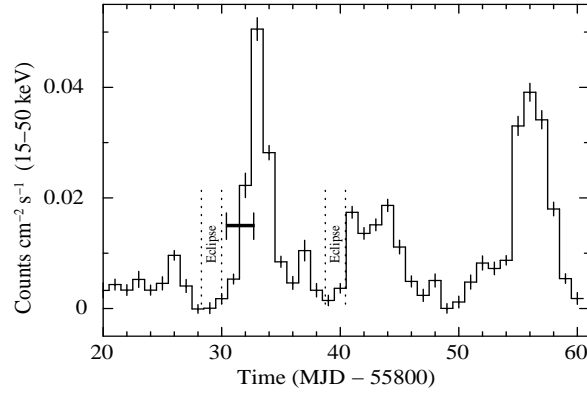


**Figure 1.** *Swift*/BAT light curve of OAO 1657-415 in 15–50 keV energy range, from 2011 September 16 (MJD 55820) to 2011 October 26 (MJD 55860). The horizontal mark shows the duration of the *Suzaku* observation of the pulsar. The durations of the eclipse are marked in the figure.

$34' \times 34'$ . The best time resolution which can be achieved in normal mode of HXD/PIN is  $61 \mu\text{s}$  (Kokubun et al. 2007).

OAO 1657-415 was observed by *Suzaku* observatory on 2011 September 26–28 for an exposure of  $\sim 85$  ks. The out-of-eclipse *Suzaku* observation of the pulsar covered about 20% of the binary orbit in 0.12–0.34 orbital phase range (considering mid-eclipse time as phase 0). The archival data of processing version 2.7.16.30 were used in the present analysis. *Suzaku* observation was carried out in “XIS nominal” pointing mode in which source is kept at the center of XIS detector. The effective exposures for XIS and HXD/PIN were  $\sim 85$  ks and  $\sim 75$  ks, respectively. XIS detectors were operated in “1/4 window mode” with a FoV of  $17'.8 \times 4'.4$  and time resolution of 2 s. *Swift*/BAT light curve of the pulsar from 2011 September 16 to 2011 October 26 is shown in Figure 1 covering the energy range in 15–50 keV. The horizontal line in the figure shows the duration of the *Suzaku* observation of the pulsar. In the figure, the duration of the eclipse, estimated by using the orbital parameters given by Jenke et al. (2012), are also marked.

Heasoft package ver 6.12 was used in the present analysis. Calibration database files released on 2012 February 10 (for XIS) and 2011 September 13 (for HXD) were used for reprocessing of *Suzaku* data. Unfiltered files were reprocessed by using the task ‘aepipeline’. Barycentric correction was applied on the reprocessed clean event files by applying ‘aebarycen’ task. Source light curves and spectra were extracted from XIS event data by considering a circular region of  $4'$  radius with source at the center, located on  $8'$  long frame of the “1/4 window” strip. Background light curves and spectra were extracted from XIS event data by considering source-free circular regions of  $2'$  radius centered at a distance of  $6'$  away the source center on the “1/4 window” strip. The response and effective area files for each XIS were generated by using tasks ‘xismfgen’ and ‘xissimarfgen’. HXD/PIN light curves and spectra of the pulsar were extracted from corresponding event files by using XSELECT package of FTOOLS. For HXD/PIN background, simulated non-X-ray background (NXB) event files corresponding to 2011 September 26

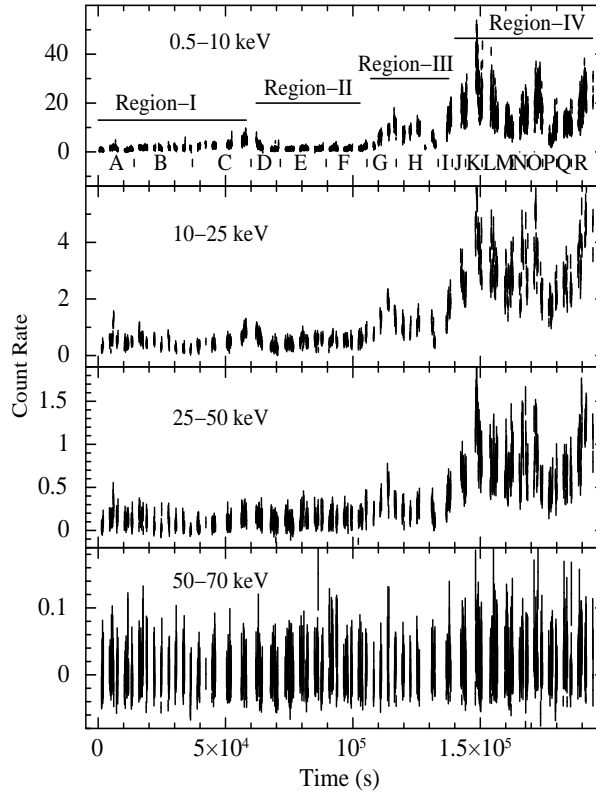


**Figure 2.** Light curves of OAO 1657-415 in 0.5-10 keV (combined data from XIS-0, 1 & 3), 10-25 keV, 25-50 keV and 50-70 keV (HXD/PIN) energy ranges obtained from the *Suzaku* observation of the pulsar in 2011 September. Depending on the variable X-ray flux during the observation, the data were divided into four broad regions as marked in the figure (top panel). The acronyms in the top panel A to R show the segments of the data used for detailed time resolution spectroscopy as described in the later part of the paper. The other panels show the presence/absence of narrow and extended low flux levels during the *Suzaku* observation. All the light curves are background subtracted.

were used to estimate the NXB<sup>1</sup> and the cosmic X-ray background was simulated as suggested by the instrument team<sup>2</sup>. The response files released on 2011 June 01 was used for HXD/PIN in the spectral analysis. Data from XIS-0, XIS-1, XIS-3 and HXD/PIN detector are used in our analysis. We have not included the GSO data due to low signal to noise ratio and high background in the hard X-ray energy ranges.

<sup>1</sup><http://heasarc.nasa.gov/docs/suzaku/analysis/pinbgd.html>

<sup>2</sup>[http://heasarc.nasa.gov/docs/suzaku/analysis/pin\\_cxb.html](http://heasarc.nasa.gov/docs/suzaku/analysis/pin_cxb.html)

### 3. Results

During the *Suzaku* observation, OAO 1657-415 was found to exhibit flux variability on several time scales. The combined XIS light curve in 0.5-10 keV range showed the presence of two extended low intensity segments and two high intensity segments as shown in Figure 2. The extended low flux segments were found in the light curves up to as high as  $\sim 50$  keV. To investigate the properties of the pulsar at different flux levels, the entire observation was divided into four broad regions and marked as Regions-I, II, III, & IV in the top panel of Figure 2. Light curves were extracted from XIS and HXD/PIN data at 2 s and 1 s time resolutions, respectively, for all four segments. The light curves were corrected for the orbital motion of the neutron star in the binary system. As the *Suzaku* observation covered about 0.2 orbital phase of the binary system, the light curves were corrected for the orbital motion by using the ephemeris given by Jenke et al. (2012). The barycentric and orbital motion corrected light curves were further used in the timing analysis of the pulsar. We have examined the energy resolved pulse profiles for all four regions by folding the corresponding background subtracted light curves on the average pulse period. It was found that pulsations were present in the light curves up to as high as  $\sim 70$  keV. The shape of the pulse profiles i.e. complex shape up to  $\sim 25$  keV because of the presence of several narrow absorption dips, were found to be similar to that reported in Pradhan et al. (2014).

To study the changes in spectral properties of OAO 1657-415 in various segments of high and low flux levels, we extracted source and background spectra from each of XIS and PIN detectors and generated corresponding response matrices as described earlier. To improve the signal-to-noise ratio, the spectral data obtained from XIS instruments were re-binned by a factor of 30 in 1.8-6 keV range, 12 in 6-8 keV range and 25 in 8-10 keV range. Similarly, HXD/PIN data were re-binned by a factor of 12 in 10-15 keV, 6 in 15-50 keV and 10 in 50-70 keV energy range. For a detailed investigation of spectral evolution of the pulsar at different flux levels during the *Suzaku* observation, we carried out the simultaneous spectral fitting of data obtained from XIS-0, XIS-1, XIS-3 and HXD/PIN in 1.8-70 keV energy range. Before spectral fitting, appropriate background subtraction was done from the data obtained from all the detectors. Because of the presence of known features of Si and Au, XIS data in 1.7-1.9 keV and 2.2-2.4 keV ranges were ignored from spectral fitting. All the model parameters were tied during spectral fitting except the detector normalizations which were kept free. In the beginning, we tried to fit the spectral data with standard continuum models such as high energy cutoff power law model, Negative and Positive power law with Exponential cutoff (NPEX) model along with interstellar absorption and iron emission line at 6.4 keV. Simultaneous spectral fitting of the XIS and HXD/PIN data during the high flux level of Region-III with high energy cutoff power law continuum model along with interstellar absorption and a Gaussian function for 6.4 keV iron emission line yielded a merely acceptable fit with a reduced  $\chi^2$  of 1.91 for 156 degrees of freedom (dof). Presence of an emission line like feature at  $\sim 7.1$  keV allowed us to add another Gaussian function to the spectral model. Addition of the second Gaussian function improved the spectral fitting further with a reduced  $\chi^2$  of 1.51 (153 dof). A blackbody component was added to the spectral model for the soft excess providing the best fit model with a reduced  $\chi^2$  of 1.19 (151 dof). The values of relative instrument normalizations of the three XISs and PIN detectors obtained from the spectral fitting are 1.00, 0.87, 0.95 & 1.14 for XIS-0, XIS-1, XIS-3 & HXD/PIN, respectively and are comparable with the values

obtained at the time of detector calibration. We attempted to fit the pulsar spectrum with NPEX continuum model along with interstellar absorption and two Gaussian functions for iron emission lines. NPEX model along with other components improved the spectral fitting marginally with a reduced  $\chi^2$  of 1.13 (151 dof). However, the value of HXD/PIN detector normalization was found to be very high (1.5). Therefore, we discarded the NPEX continuum model in our spectral fitting. While fitting the XIS and HXD/PIN spectra during all other regions, we found that the high energy cutoff power law continuum model fitted data better than NPEX continuum model. The mathematical form of the high energy cutoff power law model is:

$$I(E) = \begin{cases} E^{-\gamma} & (E \leq E_c) \\ E^{-\gamma} \exp\left(-\frac{E-E_c}{E_f}\right) & (E > E_c) \end{cases} \quad (1)$$

where  $E_c$  and  $E_f$  are cutoff energy and folding energy, respectively.

The emission line corresponding to the second Gaussian function in the spectral model was identified to be iron  $K_\beta$  fluorescent emission line. This line was found to be present in the pulsar spectrum during the *Suzaku* observation of the pulsar which has been reported by Pradhan et al. (2014). While fitting the spectra of high flux level (Region-IV), we found a weak signature of Ni  $K_\alpha$  line at 7.48 keV in the residue. Addition of a Gaussian component at 7.48 keV improved the  $\chi^2$  value from 287 (145 dof) to 262 (142 dof). The equivalent of Ni  $K_\alpha$  line was estimated to be  $23.7 \pm 3.5$  eV. This line was also detected in a few other cases such as GX 301-2 (Fürst et al. 2011; Suchy et al. 2012). In the spectral fitting, however, there was no signature of presence of earlier reported cyclotron resonance scattering feature (CRSF) at  $\sim 36$  keV (Orlandini et al. 1999). We, therefore, did not include CRSF component in the spectral fitting. Simultaneous spectral fitting of XIS and HXD/PIN data were carried out for all four regions of the *Suzaku* observation of the pulsar and shown in Figure 3. The top panels of the figure showed the spectral data along with the best-fit model components for all four regions whereas the residuals obtained from the spectral fitting without the inclusion of blackbody and 7.06 keV iron emission line in the model are shown in middle panels. The bottom panels showed the residuals obtained by adding both the components to the spectral model. The best-fit parameters (with 90% errors) obtained from simultaneous spectral fitting are given in Table 1. Among the four regions, the data during Regions-I & II were found to be significantly affected by absorption with the values of absorption column density of  $51 \times 10^{22}$  atoms  $\text{cm}^{-2}$  and  $76 \times 10^{22}$  atoms  $\text{cm}^{-2}$ , respectively. Though the flux of 6.4 keV and 7.06 keV iron emission lines were maximum during the high intensity level of Region-IV, the equivalent width of these lines were significantly high during the low flux level of Region-II. The continuum flux in 2-70 keV range were found to be comparable during Regions-I & II. For a detailed understanding of the changes in the values of absorption column density, equivalent widths and flux of iron emission lines during different regions, we attempted to do time resolved spectroscopy by dividing the entire observation into 18 narrow segments (as marked at the bottom of Figure 2). As described earlier, XIS and HXD/PIN spectra were extracted for each of the narrow segments. Previously extracted background spectra and response files were used for the spectral fitting of XIS and HXD/PIN data during these narrow segments. Simultaneous spectral fitting was carried out by using the high energy cutoff power law model along with other

**Table 1.** Best-fit parameters (with 90% errors) for the four regions.

Parameter	Value			
	Region-I	Region-II	Region-III	Region-IV
$N_H$ ( $10^{22}$ atoms $\text{cm}^{-2}$ )	51.33±4.09	75.74±5.91	24.81±1.67	28.45±0.93
Power-law index	1.04±0.12	1.12±0.07	1.16±0.07	0.98±0.04
Norm. <sup>a</sup> of Power-law ( $10^{-2}$ )	1.24±0.30	1.41±0.43	3.78±0.60	5.83±0.48
$kT_{BB}$ (keV)	0.33±0.04	0.30±0.05	0.32±0.03	0.32±0.01
Norm. <sup>b</sup> of $kT_{BB}$ ( $10^{-2}$ )	2.04±1.39	18.43±14.31	1.82±0.83	6.99±1.56
High energy cut-off (keV)	16.74±2.88	20.81±1.34	19.22±2.17	18.54±0.57
Folding energy (keV)	19.38±1.85	21.38±2.61	23.05±3.01	21.69±0.81
Fe $K_\alpha$ line Energy (keV)	6.413±0.006	6.411±0.003	6.411±0.005	6.420±0.004
Width of Fe $K_\alpha$ (keV)	0.01±0.03	0.01±0.01	0.01±0.01	0.03±0.02
Norm. <sup>c</sup> of Fe $K_\alpha$	3.92±0.28	18.74±1.40	9.20±0.46	20.94±0.55
Fe $K_\alpha$ eq. width (eV)	218.34±14.71	1069.38±79.61	211.46±10.49	221.42±5.82
Fe $K_\alpha$ line flux <sup>d</sup>	1.61±0.09	4.94±0.37	6.05±0.30	12.96±0.34
Fe $K_\beta$ line Energy (keV)	7.077±0.057	7.072±0.009	7.07 (fr)	7.112±0.038
Width of Fe $K_\beta$ (keV)	0.01±0.07	0.01±0.05	0.07±0.07	0.09±0.03
Norm. <sup>c</sup> of Fe $K_\beta$	0.82±0.10	2.89±0.23	1.73±0.66	5.79±1.03
Fe $K_\beta$ eq. width (eV)	66.94±13.89	267.40±21.60	46.93±18.02	66.08±11.78
Fe $K_\beta$ line flux <sup>d</sup>	0.47±0.10	1.18±0.10	1.28±0.49	3.72±0.66
Flux <sup>e</sup> (in 2-10 keV range)	0.38±0.09	0.28±0.07	1.61±0.25	3.32±0.30
Flux <sup>e</sup> (in 10-70 keV range)	4.67±1.44	4.46±1.35	11.49±1.81	27.10±2.22
$\chi^2$ (dof)	219 (149)	275 (148)	181 (152)	262 (142)

$N_H$  = Equivalent hydrogen column density, <sup>a</sup> : photons  $\text{keV}^{-1}\text{cm}^{-2}\text{s}^{-1}$  at 1 keV, <sup>b</sup> : in units of  $10^{39}$   $\text{erg s}^{-1} (\text{d}/10 \text{ kpc})^{-2}$  where  $d$  is distance to the source, <sup>c</sup> : in units of  $10^{-4}$  photons  $\text{s}^{-1}\text{cm}^{-2}$ , <sup>d</sup> : in  $10^{-12}$   $\text{ergs cm}^{-2} \text{s}^{-1}$  unit, <sup>e</sup> : in  $10^{-10}$   $\text{ergs cm}^{-2} \text{s}^{-1}$  unit.

components as used earlier. Iron line parameters were kept free during the spectral fitting with a lower limit of line width at 1 eV. Though, the energy and width of both Fe lines were similar during entire observation, the energy and width of Fe  $K_\beta$  line were found to be high ( $\sim 7.28$  keV and  $\sim 0.2$  keV, respectively) during segments G & K. Therefore, the values of line energy was fixed at 7.07 keV during the segments G and K. The best-fit parameters obtained from the simultaneous spectral fitting were plotted in Figure 4 along with the source light curve in 0.5-10 keV range in top panels.

The value of equivalent hydrogen column density  $N_H$  (second panel; left side of Figure 4) was found to vary in a wide range. It was maximum in the beginning of the observation for a short duration (early part of Region-I) which decreased by a factor of  $\sim 4$  and then increased again during the Region-II. Beyond Region-II, the value of  $N_H$  became low during the high flux



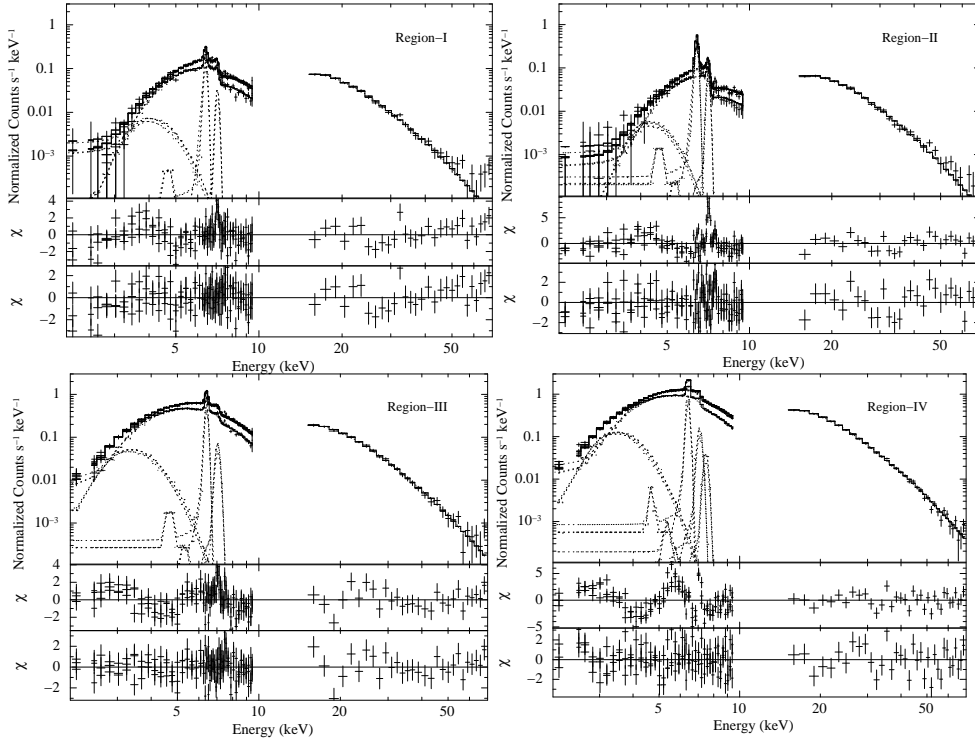


**Figure 3.** Energy spectrum of OAO 1657-415 at four different flux levels (as shown in Figure 2) during the *Suzaku* observation in 2011 September 26-28. Spectral data from XIS and HXD/PIN detectors are shown in the top panels of all four regions, along with the best-fit model comprising of a high energy cutoff power law with a blackbody component, interstellar absorption and two narrow iron emission lines at 6.4 keV and 7.06 keV. The middle panels show the contribution to the  $\chi^2$  for each energy bin for the high energy cutoff power-law model along with interstellar absorption and iron  $K_{\alpha}$  emission line. The presence of another emission line like feature at  $\sim 7.06$  keV was present in the residuals of each segments. Along with two iron emission lines, a third line at 7.48 keV which was identified as Ni  $K_{\alpha}$  line was required to fit the high flux level spectrum of Region-IV. The contributions of the residuals to the  $\chi^2$  for each energy bin for the best-fit model are shown in the bottom panels for corresponding regions.

segments of Regions-III and IV. The change in power law photon index was not significant enough (though a marginal decrease was seen towards the end of the observation; second panel - right side) to draw any conclusion on spectral state change in the pulsar. The blackbody normalization was found to be varying in similar pattern as  $N_H$  (Figure 4). However, the normalization of power law component was seen increasing along with the source flux. Though, the flux of both the iron emission lines (fifth panels from top) increased with the increase in source flux (fourth panels from top), equivalent width of these emission lines did not show any such change. The values of equivalent widths were significantly high during the low flux level of Region-II. To investigate the change in iron emission line parameters with the observed continuum flux, we plotted flux

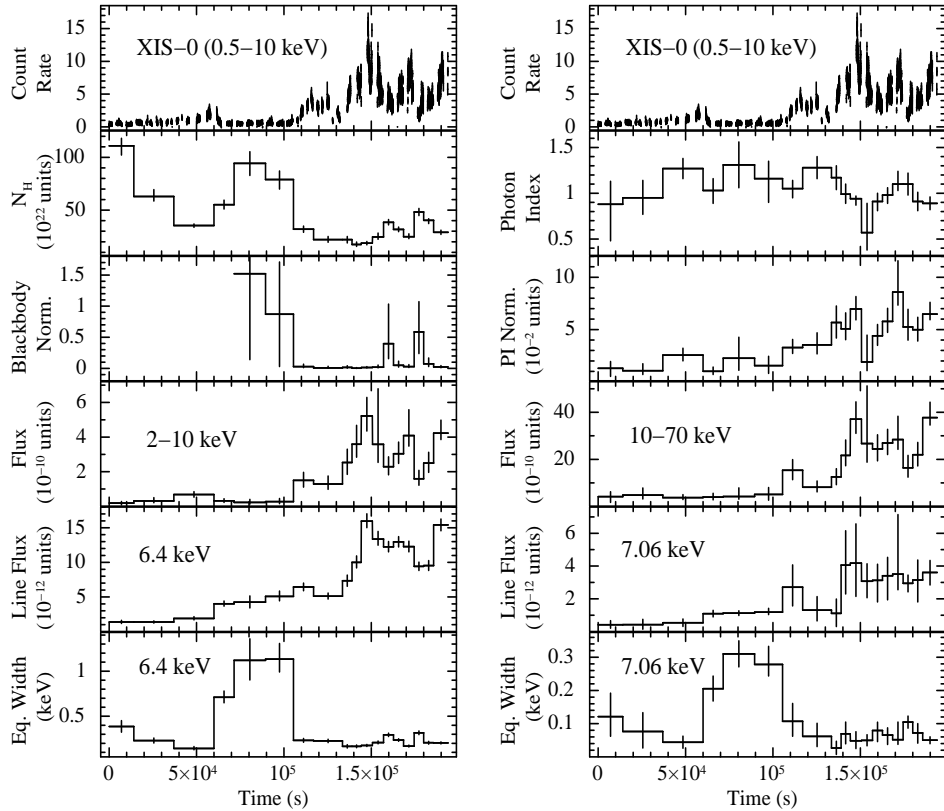


**Figure 4.** Spectral parameters obtained from the time-resolved spectroscopy of *Suzaku* observation of OAO 1657-415. The top panels in both the sides show light curves of the pulsar in 0.5-10 keV energy range. The values of  $N_H$  and power law photon index are shown in second panels in left and right side, respectively. The source flux in 2-10 keV (left side) and 10-70 keV (right side) in  $10^{-10}$  ergs  $\text{cm}^{-2}$   $\text{s}^{-1}$  units are shown in third panels. Fourth and fifth panels in both the sides show the line flux in  $10^{-12}$  ergs  $\text{cm}^{-2}$   $\text{s}^{-1}$  units and equivalent widths of 6.4 keV and 7.06 keV iron emission lines, respectively. The errors shown in the figure are estimated for 90% confidence level.

of iron emission lines and equivalent widths with respect to the total flux in 1.8-70 keV energy range (as shown in Figure 5). It was found that the flux of both the lines increased continuously with increase in the source flux though the increase was significantly high in case of 6.4 keV line. However, the equivalent width of both the lines were very high during the low flux segment of Region-II (shown in the right panel Figure 5 with larger size markers) whereas during the rest of the segments, the changes were minimal or nearly constant. Unusual high value of equivalent widths for both the iron emission lines during Region-II compared to that during Region-I, though both were at similar flux level, suggested the presence of significant amount of additional matter emitting iron emission lines at that orbital phase of the binary pulsar. More observations of

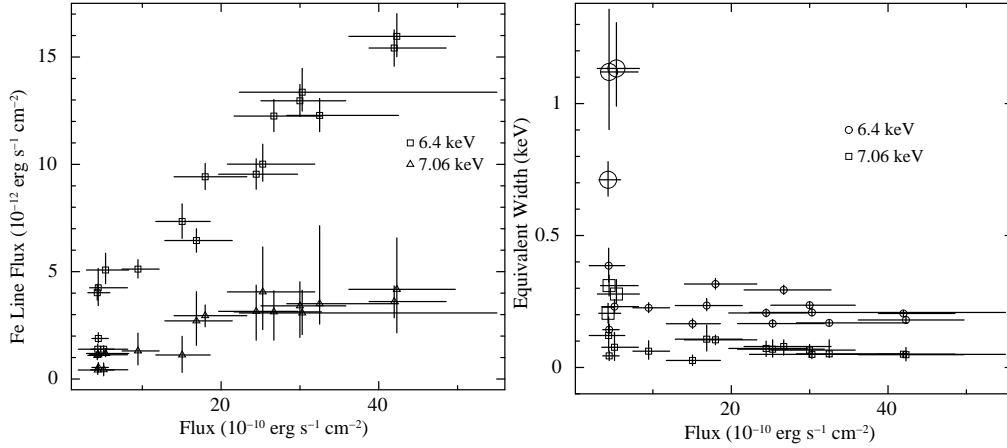


**Figure 5.** Change in the 6.4 keV and 7.06 keV iron emission line flux (left panel) and equivalent widths (right panel) with respect to the observed flux in 2-70 keV energy range. The squares and triangles in left panel represented flux for 6.4 keV and 7.06 keV iron lines, respectively. In the right panel, the circles and squares showed the equivalent widths of 6.4 keV and 7.06 keV iron lines, respectively. The markers in large sizes represented the corresponding values estimated during the low flux segment of Region-II (in Figure 2).

OAO 1657-415 with longer exposures can provide details of the matter distribution along the orbit of the binary system.

#### 4. Discussion

Photons emitted from the magnetic poles of the accretion powered X-ray pulsars interact with matter in the surrounding regions such as accretion column, accretion stream, accretion disk, dust clouds, interstellar medium before reaching the observer. These interactions are reflected in the observed spectral and timing properties of these objects. Presence of several components such as soft X-ray excess, fluorescent emission lines in the spectrum are attributed to the evidence of accretion disk formation whereas detection of cyclotron absorption features lead to the estimation of surface magnetic field of the neutron star. Fluorescent iron emission lines are seen in the spectra of most of the X-ray pulsars. X-ray photons emitted from the pulsar interact with the ionized/neutral iron atoms emitting characteristic emission lines. These interactions occur at various reprocessing sites such as the atmosphere of companion star, stellar wind stagnated in shock front, accretion disk. Therefore, the investigation of iron emission lines provides powerful tool to understand the characteristics of the accretion plasma and their spatial distribution in extreme physical conditions around the neutron star. Strength of iron emission lines depend on the continuum emission and the density/amount of available line emitting materials. The change in observed values of iron emission line parameters with a short duration over orbital phase implies the presence of inhomogeneously distributed matter over the orbit of the binary pulsar.

*Suzaku* observation of OAO 1657-415 during out-of-eclipse orbital phase in 2011 September showed the presence of 6.4 keV and 7.06 keV iron emission lines in its spectrum. Although the observed continuum flux of the pulsar was highly variable during the observation, both the lines were present in the spectrum during entire observation. However, strength of these lines were significantly different even during the extended durations of low intensity levels. During Region-II, the equivalent width of the lines were found to be  $\sim 10$  times higher than that during the other low flux segment (Region-I). The value of equivalent hydrogen column density was also found to be high during Region-II compared to that during Region-I (Table 1). Flux of both the lines was found to be directly correlated with the observed continuum flux (Figure 5). This indicates the fluorescence origin of iron lines from the cool matter surrounding the neutron star (Makishima 1986). The direct correlation between the line flux and pulsar continuum flux also suggests that the location of reprocessing region is closer to the central source.

Observed changes in the iron emission line parameters with respect to continuum flux led to the interpretation of line emitting regions in the accretion powered X-ray pulsars. Investigation of iron emission lines in the HMXB pulsar Cen X-3 during eclipse-ingress, eclipse, eclipse-egress and out-of-eclipse phases confirmed that the Fe  $K_{\alpha}$  line is being originated from regions close to neutron star whereas 6.7 keV and 6.97 keV lines are produced in a region that is far from the neutron star, probably in the highly photo-ionized wind of the companion star or in the accretion disk corona (Ebisawa et al. 1996; Naik et al. 2011; Naik & Paul 2012). Detection of pulsation in 6.4 keV iron emission line in some cases such as Vela X-1 (Choi et al. 1996), Her X-1 (Zane et al. 2004) etc. confirmed the reprocessing region to be close to the neutron star. ASCA observations of OAO 1657-415 confirmed that the origin of the 6.4 keV iron fluorescent emission line is originated from regions closer to the neutron star whereas the 6.9 keV recombination line is originated from the extended ionized stellar wind of the optical companion star (Audely et al. 2006). Dependence of iron emission line parameters with source continuum flux had also been investigated in a few X-ray pulsars such as LMC X-4 and Her X-1 (Naik & Paul 2003). A direct correlation between the flux of iron emission line and continuum flux was detected in both the pulsars whereas no systematic variation was detected in the values of equivalent width and source flux. In case of both the pulsars, the flux modulation at super-orbital periods were interpreted as due to the presence of precessing tilted accretion disk that blocks the direct X-ray beam from the pulsar. Considering the similarities in the changes in the iron line parameters with source flux in Cen X-3, LMC X-4, Her X-1, we suggest that the flux variation at different orbital phases of OAO 1657-415, as seen in the 2011 *Suzaku* observation of the pulsar, can be explained by the presence of additional dense absorbing matter at corresponding orbital phases. Further observations of OAO 1657-415 would confirm whether the segment of low flux level (due to obscuration/absorption of direct X-rays from the pulsar) repeatedly present (possibly because of the presence of structures in the close proximity of the pulsar) or a temporary one due to the presence of clump of matter.

The pulsar OAO 1657-415 showed significant flux variability during the *Suzaku* observation in 2011 September. Though the observation was carried out during out-of-eclipse phase of 10.44 d orbital period, there were two elongated segments of low flux levels followed by regions of high flux level. Similar flux variability was seen in the light curve of another HMXB pulsar

Cen X-3 (Naik et al. 2011) obtained from *Suzaku* observation in 2008 December covering nearly one orbital period. Segments of low and high flux levels occurred more frequently during the *Suzaku* observation of the pulsar. The observed changes in the source flux as well as the value of absorption column density during the *Suzaku* observation of Cen X-3 is found to be comparable to that observed during the *Suzaku* observation of OAO 1657-415.

Using the same observation used in the present work, Pradhan et al. (2014) have interpreted the flux variability of OAO 1657-415 as due to the presence of dense clump of matter at certain orbital phases. In the spectral fitting, Pradhan et al. (2014) used data from all three XIS and PIN covering in 3-70 keV range. In the present study, however, we have included the low energy data in our spectral fitting for the better estimation of the value of equivalent hydrogen column density at different orbital phases of the binary pulsar. In our fitting, the pulsar spectrum in 1.8-70 keV was well described with high energy cutoff power-law model along with other components for interstellar absorption and iron emission lines. Though, Pradhan et al. (2014) excluded data below 3 keV, partial absorbing component was required in their spectral fitting for two segments. However, in our spectral fitting in 1.8-70 keV range, the additional absorption component was not required during any of the narrow data segments shown in Figure 2. The interesting thing was the pattern of variation in the value of absorption column density was similar in both the cases (Figure 4 of our present work and Figure 8 of the work of Pradhan et al. 2014). Apart from the value of  $N_H$ , the equivalent width of both iron emission lines were found to be maximum during the second extended low segment. Though Pradhan et al. (2014) needed a cyclotron resonance scattering feature (CRSF) component in their spectral fitting to the data during both the extended low segments, no such component was required while fitting the data in the present work. Using the same *Suzaku* observation of the pulsar, here we are investigating in detail the characteristic physical parameters of the clumps causing the flares and low flux segments in the light curve.

Significant flux variability in OAO 1657-415 during *Suzaku* observation can be explained by using clumpy stellar wind model (Feldmeier et al. 2003; Oskinova et al. 2007). The accretion of clumps of matter onto the pulsar causes increase in source luminosity by producing flares/flare-like episodes in X-ray emission. The obstruction/absorption of X-ray photons by dense clumps of matter in the line-of-sight can also cause segments of low flux levels in X-ray light curve. Considering inhomogeneous distribution of matter in the stellar wind, the luminosity of such wind-powered HMXB pulsars depends on the density and velocity of the stellar wind through the relation (Bondi & Hoyle 1944)

$$L_x \propto \rho v^{-3} \quad (2)$$

where  $\rho$  is density and  $v$  is the wind velocity as described in  $\beta$ -velocity law (Castor et al. 1975). Any fluctuation in either density or velocity profile produces the time variability in the source luminosity.

The clumpy wind model can explain the observed variability in circumstellar absorption and source flux. The physical parameters of the clumpy wind can be estimated from the observed time variability in the light curve of OAO 1657-415 using this model. Figure-2 shows the presence of a series of flares of duration of  $\geq 10$  ks. Considering a flare of duration  $t_f \sim 10$  ks and relative wind velocity  $v_{rel} \sim 250 \text{ km s}^{-1}$  (taking an approximation of terminal velocity similar to the relative

velocity; Mason et al. 2012), the radius of the clump can be

$$R_c \simeq \frac{v_{rel} t_f}{2} = 1.25 \times 10^{11} \left( \frac{v_{rel}}{250 \text{ km s}^{-1}} \right) \left( \frac{t_f}{10 \text{ ks}} \right) \text{cm} \quad (3)$$

Gravitational influence of the neutron star on the clumps becomes effective at the accretion radius  $r_{acc} \sim 2GM_{ns}/v_{rel}^2$ . As a clump of matter crosses this radius, it gets accreted toward the neutron star. The accretion radius for OAO 1657-415 is calculated to be  $\sim 6 \times 10^{11}$  cm by assuming typical parameters of the neutron star and relative stellar wind velocity of  $250 \text{ km s}^{-1}$ . Accretion radius also imposes a constrain on upper limit of the radius of a clump that can be accreted entirely onto the neutron star. Mass of the accreted clump can be estimated by comparing the gravitational potential energy of clump to the energy released due to its accretion onto the neutron star (assuming efficiency  $\eta$  as 0.1) through the relation (Zel'dovich & Shakura 1969)

$$M_c = \frac{L_x t_f R_{ns}}{\eta G M_{ns}} = 5 \times 10^{21} \left( \frac{L_x}{10^{37} \text{ erg s}^{-1}} \right) \left( \frac{t_f}{10 \text{ ks}} \right) \text{g} \quad (4)$$

where  $M_{ns}$ ,  $R_{ns}$  and  $L_x$  are mass, radius and X-ray luminosity of the neutron star, respectively. Therefore, for a given set of physical parameters of the spherical clump, its mean density ( $n_c$ ) and radial column density ( $N_c$ ) can be estimated as

$$n_c = \frac{3M_c}{4\pi m_p R_c^3} = 4 \times 10^{11} \left( \frac{L_x}{10^{37} \text{ erg s}^{-1}} \right) \times \left( \frac{t_f}{10 \text{ ks}} \right)^{-2} \left( \frac{v_{rel}}{250 \text{ km s}^{-1}} \right)^{-3} \text{cm}^{-3} \quad (5)$$

$$N_c = n_c R_c = 5 \times 10^{22} \left( \frac{L_x}{10^{37} \text{ erg s}^{-1}} \right) \times \left( \frac{t_f}{10 \text{ ks}} \right)^{-1} \left( \frac{v_{rel}}{250 \text{ km s}^{-1}} \right)^{-2} \text{cm}^{-2} \quad (6)$$

Using the typical parameters in equation (5), the mean density of a clump can be estimated to be  $4 \times 10^{11} \text{ cm}^{-3}$ . However, the mean number density of the stellar wind around the neutron star is calculated to be  $n \sim 4 \times 10^{10} \text{ cm}^{-3}$  by using the  $\beta$ -velocity law (Castor et al. 1975) and the wind parameters from Mason et al. (2012). Stellar wind density is found to be an order of magnitude lower than the value obtained from equation (5).

In the present *Suzaku* observation, the duration and luminosity of the flare (segments G & H) are about  $\sim 25$  ks and  $0.66 \times 10^{37} \text{ erg s}^{-1}$ , respectively. Using these values in Equation 6, the clump column density ( $N_c$ ) is estimated to be  $1.3 \times 10^{22} \text{ cm}^{-2}$ . However, the difference in the observed value of  $N_H$  (from spectral fitting) for segments F (prior to the flare) and G & H (during flare) is found to be  $52 \times 10^{22} \text{ cm}^{-2}$ . This value corresponds to the column density of clump that produced a flare of  $\sim 25$  ks duration (segments G & H). However, it is found to be  $\sim 40$  times more than the expected column density ( $N_c$ ). In case of another flare (segments I to L) with duration of  $\sim 24$  ks and luminosity of  $1.38 \times 10^{37} \text{ erg s}^{-1}$ , the clump column density ( $N_c$ ) is estimated to be  $2.9 \times 10^{22} \text{ cm}^{-2}$ . From spectral fitting, the difference in  $N_H$  between the flare (segments from

I to L) and the segment prior to the flare (segment H) is calculated to be  $1.4 \times 10^{22} \text{ cm}^{-2}$  which is comparable to the estimated value  $N_c$ . For the flare starting from segment N to segment P, the duration and luminosity are  $\sim 12 \text{ ks}$  and  $1.31 \times 10^{37} \text{ erg s}^{-1}$ , respectively. Using these values, the clump column density ( $N_c$ ) is estimated to be  $5.4 \times 10^{22} \text{ cm}^{-2}$ . However, as calculated earlier, the clump density from spectral fitting is found to be  $3.6 \times 10^{22} \text{ cm}^{-2}$  which is also close to  $N_c$ . From these examples, it is found that the values of observed and calculated clump column densities are comparable. This supports the suggestion that the observed flux variability in the pulsar light curve can be explained by using clumpy wind hypothesis.

However, in case of the flare during segments G & H, the estimated clump column density from spectral fitting is quite high compared to the expected column density calculated by using Equation 6 in case of a spherically symmetric clump of homogeneous density. The enhancement in the value of column density compared to the standard wind density can occur because of the instability in variable and highly structured stellar wind. As the supersonic stellar wind interacts with the neutron star, a bow shock of compressed gas forms near  $r_{acc}$  that may cause enhancement in the column density. Numerical simulation results for the wind-fed sources indicate that the regions inside the non-steady accretion wake consist of dense filaments in which the density reaches up to  $\sim 100$  times more as compared to undisturbed stellar wind (Blondin et al. 1990). Such dense clump or filament can absorb the X-ray photons up to higher energies and results the low flux levels in the light curve.

Interaction of X-ray photons either in dense filaments or stagnated shock front can contribute to higher value of the equivalent width. Inoue (1985) performed Monte Carlo simulation for the fluorescence emission from the neutral atom as a function of absorber density. Different model components were considered in the above study. A model with a combination of direct and scattered continuum component explained the possibility of high equivalent width (up to order of keV) with variation in  $N_H$ . If the absorbing matter situated directly between the observer and the X-ray source, then the equivalent width for emission lines was found to be monotonically proportional to the column density. As a result the high equivalent width (more than 100 eV) for 6.4 keV line was seen at  $N_H > 10^{23} \text{ cm}^{-2}$ .

In summary, we interpret our results based on the clumpy wind hypothesis. The extended low flux levels of Region-I & II can be interpreted as the presence of dense clump or filament of the compressed gas. The high equivalent width of Fe  $K_\alpha$  and Fe  $K_\beta$  lines can be understood by the result obtain from Monte Carlo simulation (Inoue 1985) in which the dense clump of matter obscures the direct X-rays and contributes to the high value of equivalent width as observed in Region-II. During the orbital phase 0.19-0.24 (Region-II), the clump could be situated along the line-of-sight. As the clump passes Region-II the absorption column density decreases and causes decrease in the equivalent width of iron emission lines. Lifetime of this clump can be similar to duration of Region-II. Furthermore, decrease in the absorption column density and increase in the source flux in Region-III & Region-IV suggest the obstruction or either the accretion of matter by relatively low dense or off line clumps.

#### 4.1 Location of the Fe fluorescence line-emitting region

To investigate the ionization state of matter (iron) in line emitting region, the ratio of Fe  $K_\beta$  line flux to that of Fe  $K_\alpha$  line was calculated for the entire *Suzaku* observation of OAO 1657-415. It was found that the value of flux ratio varies between  $0.15 \pm 0.11$  and  $0.42 \pm 0.18$  for all segments. The value of line flux ratio for each segment was found to be higher than the theoretically predicted value ( $\sim 0.13$ ) for neutral iron atom in optical thin medium (Kaastra & Mewe 1993; Palmeri et al. 2003; Han & Demir 2009). This suggests that the line emitting region can be a mixture of neutral and ionized iron atoms. The observed line energy and flux ratio indicate the possible existence of ionized iron atoms in ionization state between Fe VIII to Fe XVIII (Palmeri et al. 2003; Mendoza et al. 2004 and Kallman et al. 2004). Ionization of the iron atoms is characterized by the ionization parameter  $\xi = L/nr^2$  and its value should be  $\xi \sim 10^{2.5}$  erg cm s $^{-1}$  for ionization state below Fe XVIII (Tarter et al. 1969; Ebisawa et al. 1996). However, the iron atoms are expected to be fully ionized at  $\xi \geq 10^3$  erg cm s $^{-1}$  (Kallman & McCray 1982). The peak population of ion at Fe XVIII can be expected to be  $\sim 0.25$  (Ebisawa et al. 1996). For a luminosity of  $10^{37}$  erg s $^{-1}$  and column density of  $10^{23} \leq N_H \leq 10^{24}$  cm $^{-2}$ , the location of ionization region is found to be in range of  $(0.3-3) \times 10^{11}$  cm from the neutron star. Using this method, we found that the location of iron ionization region lies within or closer to the accretion radius  $r_{acc}$ . Our result agrees with that obtained from earlier studies in which the location of iron fluorescence region was estimated to be within the region of  $5.7 \times 10^{11}$  cm (19 lt-sec) (Audley et al. 2006).

## 5. Conclusions

We have analyzed the timing and spectral properties of OAO 1657-415 during a long *Suzaku* observation in 2011 September. The pulsar was found to be exhibiting low and high flux levels during the observation. The segments of low flux levels are seen up to as high as  $\sim 50$  keV in the light curves of the pulsar. The spectrum of the pulsar in 1.8-70 keV range was found to be well described by the high energy cutoff model. Iron fluorescent emission lines at 6.4 keV and 7.06 keV were detected in the spectrum of the pulsar through out the low and high flux levels. Flux of the iron emission lines was found to be variable with the continuum flux whereas the equivalent width was nearly constant with flux except for Region-II. The correlation between observed line flux and continuum flux suggests the fluorescent origin of the iron lines from the regions near to the neutron star. It is evident from the line energy and flux ratios of Fe  $K_\beta$  and Fe  $K_\alpha$  lines that line emitting regions consist of a mixture of neutral and ionized iron atoms. We estimated distance of the fluorescence region and found that region lies within the accretion radius. Considering the high value of absorption density during the segments of low flux level and high values of iron line equivalent widths, we can explain that the low flux segments in OAO 1657-415 are due to the presence of dense clumpy matter at certain orbital phases of the binary system.



## Acknowledgments

We thank the referee for her/his constructive comments and suggestions that improved the content of the paper. The research work at Physical Research Laboratory is funded by the Department of Space, Government of India. The authors would like to thank all the members of *Suzaku* for their contributions in the instrument preparation, spacecraft operation, software development, and in-orbit instrumental calibration. This research has made use of data obtained through HEASARC Online Service, provided by NASA/GSFC, in support of NASA High Energy Astrophysics Programs.

## References

- Audley M. D., Nagase F., Mitsuda K., Angelini L., Kelley R. L., 2006, MNRAS, 367, 1147  
Barnstedt J., Staubert R., Santangelo A., et al., 2008, A&A, 486, 293  
Baykal A., 1997, A&A, 319, 515  
Baykal A., 2000, MNRAS, 313, 637  
Bildsten L., Chakrabarty D., Chiu J., et al., 1997, ApJS, 113, 367  
Blondin J. M., Kallman T. R., Fryxell B. A., Taam R. E., 1990, ApJ, 356, 591  
Bondi H., Hoyle F., 1944, MNRAS, 104, 273  
Castor J. I., Abbott D. C., Klein R. I., 1975, ApJ, 195, 157  
Chakrabarty D., Grunsfeld J. M., Prince T. A., et al., 1993, ApJ, 403, L33  
Chakrabarty D., Wang Z., Juett A. M., Lee J. C., Roche P., 2002, ApJ, 573, 789  
Choi C. S., Dotani T., Day C. S. R., Nagase F., 1996, ApJ, 471, 447  
Corbet R. H. D., 1986, MNRAS, 220, 1047  
Ebisawa K., Day C. S. R., Kallman T. R., et al., 1996, PASJ, 48, 425  
Feldmeier A., Oskinova L., Hamann W., 2003, A&A, 403, 217  
Fürst F., Suchy S., Kreykenbohm I., et al., 2011, A&A, 535, 9  
Han I., Demir L., 2009, Phys. Rev. A, 80, 052503  
Inoue H., 1985, Space Sci. Rev., 40, 317  
Jenke P. A., Finger M. H., Wilson-Hodge C. A., Camero-Arranz A., 2012, ApJ, 759, 124  
Kaastra J. S., Mewe R., 1993, A&AS, 97, 443  
Kallman T. R., McCray R. 1982, ApJ, 50, 263  
Kallman T. R., Palmeri P., Bautista M. A., et al., 2004, ApJS, 155, 675  
Kamata Y., Koyama K., Tawara Y., et al., 1990, PASJ, 42, 785  
Kokubun M., Makishima K., Takahashi T., et al., 2007, PASJ, 59, 53  
Koyama K., Tsunemi H., Dotani T., et al., 2007, PASJ, 59, 23  
Makishima K., 1986, The Physics of Accretion onto Compact Objects, ed. K. P. Mason, M. G. Watson, N. E. White, Lecture Notes in Physics, Berlin: Springer, 266, 249  
Mason A. B., Clark J. S., Norton A. J., Negueruela I., Roche P., 2009, A&A, 505, 281  
Mason A. B., Clark J. S., Norton A. J., et al., 2012, MNRAS, 422, 199  
Mendoza C., Kallman T. R., Bautista M. A., Palmeri P., 2004, A&A, 414, 377  
Mitsuda K., et al., 2007, PASJ, 59, 1  
Naik S., Paul B., 2003, A&A, 401, 265  
Naik S., Paul B. 2012, BASI, 40, 503  
Naik S., Paul B., Ali Z., 2011, ApJ, 737, 79  
Orlandini M., dal Fiume D., del Sordo S., et al., 1999, A&A, 349, L9

- Oskinova L. M., Hamann W., Feldmeier A., 2007, *A&A*, 476, 1331  
Palmeri P., Mendoza C., Kallman T. R., et al., 2003, *A&A*, 410, 359  
Parmar A. N., Branduardi-Raymont G., Pollard G. S. G., et al., 1980, *MNRAS*, 193, 49  
Pradhan P., Maitra C., Paul B., Islam N., Paul B. C., 2014, *MNRAS*, 442, 2691  
Polidan R. S., Pollard G. S. G., Sanford P. W., Locke M. C., 1978, *Nature*, 275, 296  
Suchy S., Fürst F., Pottschmidt K., et al. 2012, *ApJ*, 745, 124  
Takahashi T., Keiichi A., Endo M., et al., 2007, *PASJ*, 59, 35  
Tarter C. B. Salpeter E. E., 1969, *ApJ*, 156, 953  
White N. E., Pravdo S. H., 1979, *ApJ*, 233, L121  
Zane S., Ramsay G., Jimenes-Garate M. A., et al., 2004, *MNRAS*, 350, 506  
Zel'dovich Ya. B., Shakura N. I., 1969, *SvA*, 13, 175